THE JOURNAL OF PHYSICAL CHEMISTRY B

ARTICLE

pubs.acs.org/JPCB

Volumetric Properties of Hydrated Peptides: Voronoi−Delaunay Analysis of Molecular Simulation Runs

Vladimir P. Voloshin,[†] Nikolai N. Medvedev,[*,†,‡] Maximilian N. Andrews,[§] R. Reddy Burri,[§] Roland Winter,[§] and Alfons Geiger[*,§]

[†]Institute of Chemical Kinetics and Combustion, SB RAS, 630090 Novosibirsk, Russia

[‡]Novosibirsk State University, 630090 Novosibirsk, Russia

[§]Physikalische Chemie, Technische Universität Dortmund, 44221 Dortmund, Germany

ABSTRACT: The study of hydration, folding, and interaction of proteins by volumetric measurements has been promoted by recent advances in the development of highly sensitive instrumentations. However, the separation of the measured apparent volumes into contributions from the protein and the hydration water, $V_{app} = V_{int} + \Delta V$, is still challenging, even with the detailed microscopic structural information from molecular simulations. By the examples of the amyloidogenic polypeptides hIAPP and Aβ42 in aqueous solution, we analyze molecular dynamics simulation runs for different temperatures, using the Voronoi−Delaunay tessellation method. This method allows a parameter free determination of the *intrinsic* volume V_{int} of complex solute molecules without any additional assumptions. For comparison, we also use fused sphere calculations, which deliver van der Waals and solute accessible surface volumes as special cases. The *apparent* volume V_{app} of the solute molecules is calculated by different approaches, using either a traditional distance based selection of hydration water or the construction of sequential Voronoi shells. We find an astonishing coincidence with the predictions of a simple empirical approach, which is based on experimentally determined amino acid side chain contributions (*Biophys. Chem.* **1999**, *82*, 35). The intrinsic volumes of the polypeptides are larger than their apparent volumes and also increase with temperature. This is due to a negative contribution of the hydration water ΔV to the apparent volume. The absolute value of this contribution is less than 10% of the intrinsic volume for both molecules and decreases with temperature. Essential volumetric differences between hydration water and bulk water are observed in the nearest neighborhood of the solute only, practically in the first two Delaunay sublayers of the first Voronoi shell. This also helps to understand the pressure dependence of the partial molar volumes of proteins.

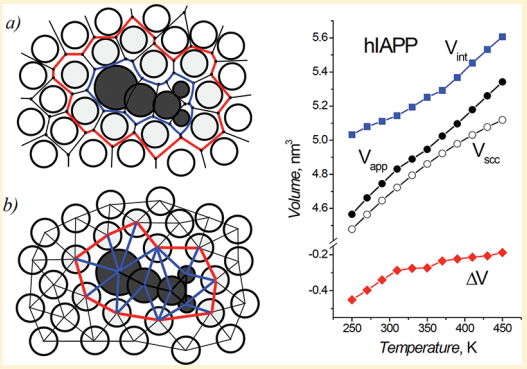

1. INTRODUCTION

Understanding of the conformation and stability of proteins has fascinated biophysicists and biochemists for many years and remains still one of the most challenging issues in the field. In general, the conformation and thermodynamic properties of proteins depend on temperature, pressure, their hydration capacity, and the solvent properties.[1,2] In this regard, one physical chemical property of proteins that has received considerably less attention over the years is the partial molar volume and its coefficient of thermal expansion, which have proven to be sensitive measures of hydration effects.[1−6] Indeed, the factors contributing to the volumetric properties of proteins and their temperature dependence have long eluded understanding. Generally, the volume of protein solutions varies with temperature due to variations in either the volume of the protein, the volume of the bulk water, the volume of the hydrating water, and/or a change in the number of interacting and bulk water molecules. How many water layers with properties different from bulk water may form at the protein surface depends on several factors: the hydrophobicity/hydrophilicity of the surface groups, the charge density and its spatial distribution, and the strength of the thermal forces that tend to disrupt the induced solvent structure. Increase of temperature is expected to lead to a disruption of the solvent layer, which, in turn, should be reflected in the temperature dependence of the expansion coefficient. Recently, a rather new technique, pressure perturbation calorimetry (PPC), has been introduced, which is complementary to densimetric measurements and has the high sensitivity which is necessary to detect small volumetric changes.[7−13] To yield a molecular interpretation of the different terms contributing to the partial protein volume and its temperature dependence, and hence a better understanding of the experimental data, molecular dynamics (MD) computer simulations and proper extraction of volumetric data are prerequisite.

To determine the properties of hydration water from molecular simulations, usually simple geometric definitions of the hydration

Special Issue: H. Eugene Stanley Festschrift

Received: May 31, 2011
Revised: August 17, 2011
Published: October 14, 2011

shell are used: the hydration shell of a dissolved molecule comprises all water molecules within some cutoff distance R from the solute molecule. The distance is measured between the oxygen atom of the water molecule and the closest heavy (non-hydrogen) atom of the solute. In this way, local properties of the hydration water, like molecular orientations, hydrogen bond network structure, dynamical properties, and thermodynamic characteristics, are calculated as averages over the water molecules within the hydration shell volume.[14−21] By varying the cutoff distance R, the sensitivity of the obtained results from the specific choice of this parameter can be tested. However, when trying to calculate volumetric properties, like the molecular volume of the solute or the hydration shell volume itself, this approach is of limited use. For example, to calculate the *intrinsic* volume of the solute molecule (the volume occupied by the molecule itself), different definitions could be used, in particular the volume within the van der Waals (vdW) surface of the molecule or within the solvent accessible surface (SAS), leaving the question of how to partition the intermediate volume between solute and solvent.

An alternative approach to define the hydration shell of a solute molecule is based on the Voronoi−Delaunay method. This method is well established in mathematics[22] and physics[23] and has been suggested for the determination of molecular structures and volumes in molecular biology.[24−27] The idea to use this method also for the construction of hydration shells is obvious: a Voronoi−Delaunay tessellation (mosaic) assigns to each atom in an atomic system an associated volume, called the *Voronoi polyhedron, Voronoi region,* or *Voronoi cell*. This cell defines not only the volume "belonging to this atom" but also its nearest neighbors: they share a common polyhedron face with the given atom. Thus, they represent a natural shell around the solute molecule. David and David[28] suggested this for a polyatomic solute. They defined the Voronoi region of a solute as the union of all Voronoi polyhedra which are centered on an atom of the solute and which are constructed by using all (heavy) atoms of the solute and all oxygen atoms of the solvent water. They considered so-called ordinary (classical) Voronoi polyhedra, which are defined for a system of points (here the centers of the atoms).[29,30] Mezei[31] pointed out that the different sizes of the atoms should be taken into account for the calculation of the Voronoi regions for molecular solutions, and proposed to use for molecular solutions so-called *radical* (*power*) Voronoi cells,[32] which are based on the atomic van der Waals spheres. Up to now, the Voronoi−Delaunay method was used only rarely for the analysis of molecular hydration shells. Indeed, if the main goal is the determination of nearest neighbors of a solute molecule, the distance based (DB) criterion is much simpler and sufficient for many purposes. Working with Voronoi regions is rather intricate in comparison with the much simpler calculation of distances between points. However, the Voronoi−Delaunay method has many advantages: First, it uses common geometrical relations to determine the nearest neighbors. There is no necessity to introduce a more or less arbitrary cutoff distance R as in the case of the DB criterion; thus, it is parameter free.[33−38] It also provides a plausible definition of the intrinsic volume. Unlike the molecular (or van der Waals) volume, the Voronoi volume does take into account structural changes which alter the free volume accessible to the solute molecule. This is a reasonable measure for comparison with the experimental values.[39−41] Moreover, the idea to use the volume which is "assigned" to the atoms can be applied not only to the solute molecule but also to the solvent. This allows the calculation of the volume of the hydration shell.[42]

Thus, the Voronoi−Delaunay method can be considered as an alternative to the traditional DB approach, both for the selection of the hydration water and for the analysis of the hydration shell characteristics. In this paper, we apply two variants of this method for the determination of the volumetric properties of the polypeptides hIAPP and Aβ42 from molecular dynamic simulations of their monomolecular aqueous solutions.

2. METHODS

2.1. MD Simulation Outline. Single amyloidogenic polypeptide chains in aqueous solution have been simulated by use of the molecular dynamics software package GROMACS 3.3.1.[43] They have the following sequences of 37 and 42 residues (one letter symbols for the amino acids[44]):

KCNTATCATQRLANFLVHSSNNFGAILSSTNVGSNTY (hIAPP) and

DAEFRHDSGYEVHHQKLVFFAEDVGSNKGAIIGLMVGGVVIA (Aβ42)and are immersed in 7407 (hIAPP) and 7704 (Aβ42), respectively, water molecules in a cubic box with periodic boundary conditions. For the peptides, the OPLS-AA force-field[45,46] has been used, and for water, the SPC/E model.[47] hIAPP is simulated in its oxidized form, with a disulfide bond.[48] The terminating groups are considered to be fully ionized. Also, the charges of the residues K, R, D, and E have been set to +1e and −1e, respectively, yielding a net charge of +2e for hIAPP and −3e for Aβ42.[21,48] In order to neutralize the system in solution, the total charge on the biopolymers was scaled down to neutrality by distributing an equal and opposite charge on all atoms of the polypeptide itself, as described in previous studies.[21,49,48] The simulation runs were performed with 2 fs time steps in the *NPT* ensemble at constant pressure p = 1 bar. More technical details on the simulation runs can be found for hIAPP in refs 48 and 64 and for Aβ42 in ref 21. Production runs of 200−500 ns each were performed for 11 different temperatures from 250 to 450 K (for the hIAPP solution) and for 22 temperatures from 250 to 460 K (for the Aβ42 solution).

For the analysis of the hIAPP solutions, 1000 independent configurations, equally spaced over the last 200 ns (every 200 ps) of the equilibrated production run, were used for averaging. (As test runs showed, averaging over 5000 and 20000 configurations (every 40 and 10 ps) yields the same results.) For the analysis of the Aβ42 solution, 1000 independent configurations (every 10 ps) were used.

2.2. Voronoi−Delaunay Method for Solvation Shells. In an atomic system, a region of space can be assigned to each atom (called here its *Voronoi cell*) which is defined such that all space points of this region are closer to the given atom than to any other atom of the system. The Voronoi cells divide the space between the atoms without gaps and overlapping, and represent the so-called *Voronoi tessellation.*

If the distance to an atom is measured to its center (the van der Waals radius of the atom not being taken into account), then one gets an *ordinary* Voronoi tessellation, defined for a system of discrete points (atomic centers).[29,30] Dashed lines show such an ordinary cell for the central atom in Figure 1. In 3D, the Voronoi cell has flat faces and is called a Voronoi polyhedron. Note, the bisector dividing the space between two centers is a plane. The points of one half-space are closest to one center, and the points of the second half-space are closer to the second center. The *intersection* of all such half-spaces for a given center gives the

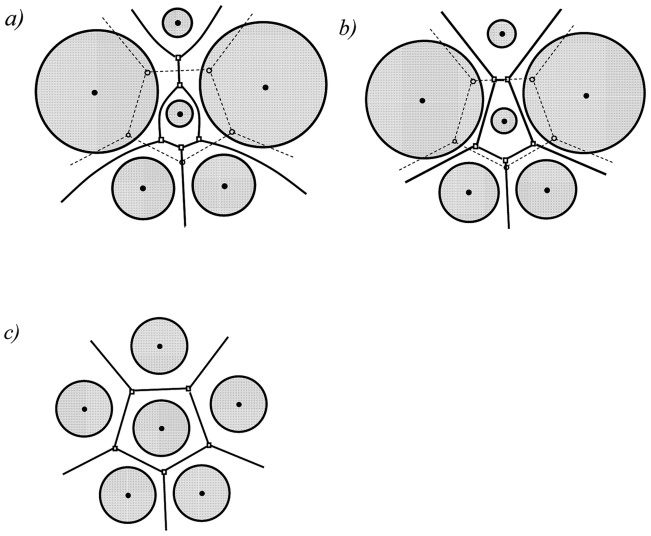

Figure 1. Illustration of Voronoi cells of different types: (a) ordinary cell (dashed lines), *S*-cell (solid lines); (b) ordinary cell (dashed lines), radical or power cell (solid lines); (c) in the case of equal atoms, all types of the Voronoi cells are identical (solid lines).

required Voronoi cell: the points of this intersection are closer to the given center than to any other center of the system.

However, the distance to an atom can also be measured to the atomic surface. In this case, the Voronoi cell can be different. From a mathematical point of view, different distance measures yield different realizations of the Voronoi tessellation.[22]

If the distance to an atom (sphere) is measured by the usual Euclidean measure to its surface (to the closest point), then the bisector for two atoms of different radii is a quadric surface (hyperboloid or ellipsoid). Thus, the faces of such Voronoi cells are not flat in general; see Figure 1a. In this paper, we will call them *Voronoi S-cells* (or simply *S-cells*). The letter S emphasizes that we deal with surfaces of atoms.[51,52] In mathematics, such a tessellation is also called an *additively weighted* Voronoi diagram.[22]

The size of atoms can also be taken into account by using so-called *power* (or *radical*) Voronoi cells[22,32,53] (Figure 1b). In this case, the bisector between two spheres is the *radical* plane, well-known in geometry. It is the locus of points having equal *power* with respect to two spheres. Here, *power* is the distance from a point in space to the point on the surface of a sphere, where the tangent from the point to the sphere is touching it. We will call this Voronoi cell a *Voronoi P-cell* (or simply *P-cell*). The advantage of the *P*-cells is that they have plane faces. It facilitates their calculation and analysis in comparison with *S*-cells. On the other hand, the physical meaning of the *P*-cells is not very clear. Some points of such a cell are really closer to another atom than to a given one. The main geometrical properties of the power tessellation are the same as for *S*-cells and the ordinary ones. Note, for systems of atoms with equal radii, all of these types of Voronoi tessellation are identical, Figure 1c.

Irrespective of the type of Voronoi cell, it can be used for the definition of neighbors. The *nearest* (*geometrical* or *first topological*) neighbors have a common Voronoi face. They present the *first Voronoi shell* around a given atom. The second and following Voronoi shells can be determined in the same way (Figure 2): The atoms of the second one are adjacent to atoms of the first one but not to the central atom. The atoms of the third one are adjacent to the second one but not to the first, and so on.

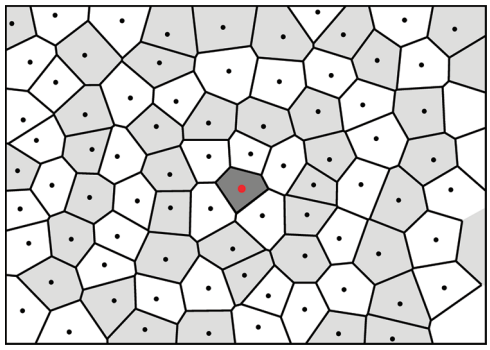

Figure 2. Illustration of Voronoi shells around a central cell.

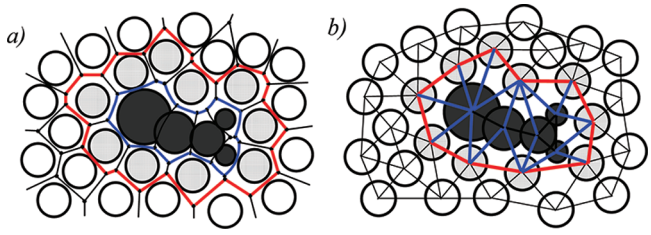

Figure 3. (a) Voronoi tessellation of a solution. The solute molecule is shown by a cluster of dark disks. The first Voronoi shell of the solute is defined by the set of its geometrical neighbors (gray solvent atoms). The union of the Voronoi cells of the solute atoms determines the Voronoi region of the solute molecule (blue lines). The union of Voronoi cells of the nearest neighbors determines the volume of the first Voronoi shell (between red and blue lines). (b) Delaunay tessellation of the same solution. The edges of the Delaunay simplexes are drawn. All atoms of the first Voronoi shell are vertexes of Delaunay simplexes which also include atoms of the solute molecule as vertex. These simplexes define the first simplicial layer around the solute.

In other words, the atoms in the *k*th Voronoi shell are the *k*th topological neighbors of the central atom on the Delaunay network. Remember, intimately connected with the Voronoi tessellation is the tessellation by *Delaunay simplexes*. The adjacency of two Voronoi cells defines a Delaunay simplex edge as the line between these atoms. In two dimensions, Delaunay simplexes are triangles (see Figure 3b), and in three dimensions, tetrahedra.

Any complex molecule is composed of atoms. The union of the Voronoi cells of these atoms defines the space assigned to a given molecule in solution (*Voronoi region of the molecule*; in section 3.3, we will identify this volume as the intrinsic volume V_{int} of the solute). According to the above considerations, this can be the ordinary, *P*- or *S*-region of the molecule. Figure 3a illustrates the *S*-tessellation of a model solution. The solute molecule is shown as a cluster of dark disks, and the nearest neighbors are marked in gray. Common faces between discs of different radii are curved. However, far from the solute, the *S*-cells of the solvent molecules coincide with ordinary Voronoi polyhedra because all of them have identical radii.

The nearest neighbors of a complex solute molecule are defined as above. They are the solvent molecules whose Voronoi cells are adjacent to the Voronoi region of the solute: gray disks around the solute in Figure 3. They represent the first Voronoi shell of the solute. In the same way, the subsequent Voronoi shells can be defined.

Apart from Voronoi cells, one can use also Delaunay simplexes to describe hydration shells. The vertexes of the simplexes are

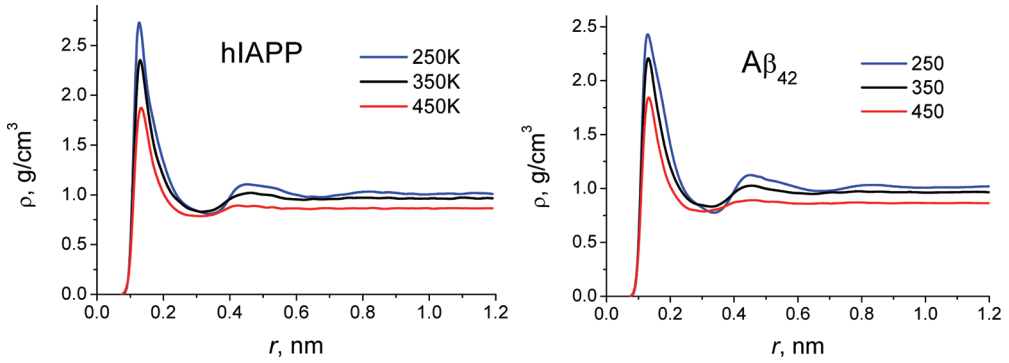

Figure 4. Water density distribution around the solute molecules hIAPP and Aβ42. Distance is measured to the surface of the nearest heavy atom. Selected curves are given for temperatures 250, 350, and 450 K.

defined by the atoms. Those simplexes, where some of the vertexes are atoms of water molecules in the first Voronoi hydration shell and others are atoms of the solute molecule, represent the *first simplicial layer* around the solute (Figure 3b). In a similar manner, using subsequent Voronoi shells, one can define the subsequent simplicial layers (see section 3.1.3).

3. RESULTS AND DISCUSSION

3.1. Structure of the Hydration Shell. *3.1.1. Density Distribution.* Figure 4 shows the density distribution function $\rho(r)$ for water around our solute molecules. The distances r are calculated from the center of the oxygen of the water molecules to the surface of the nearest heavy atom of the solute molecule (distance to the center of the atom minus its van der Waals radius $\sigma_{AA}/2$, so this differs from the usual atom−atom pair distribution functions). As in the whole paper, for the size of the spheres, representing the atoms, we use the Lennard-Jones σ from the simulation force field. The behavior of $\rho(r)$ is typical for moderately hydrophilic walls:[50,54] a clear first peak around 0.14 nm, and a second at about 0.45 nm, followed by damped oscillations.

To calculate $\rho(r)$, we sum up the masses of the water molecules $N(r)$ in layers of thickness dr at distance r from the molecular surface, and normalize by the current volume d$V(r)$ of the layers, as in the calculation of ordinary radial pair correlation function $g(r)$. However, here we deal with nonspherical solute molecules and layers. Besides, the shape of the molecule is changing during the simulation. This means that we have to calculate the value d$V(r)$ explicitly every time. We have done this by the overlapping spheres construction, discussed in section 3.3. Naturally, at large distances, the curves in Figure 4 approach the density of bulk water in the solution at the given temperature.

Figure 5 shows the obtained density of the bulk water for the Aβ42 solution as a function of temperature. Here, water molecules beyond 0.8 nm from the solvent molecule were referred to as bulk water. The density approaches its maximum slightly below 250 K, as is known from pure SPC/E water simulations.[55] The mean volume of the water Voronoi cells, $\langle V_{VP}\rangle$, for the bulk water is also presented in the figure. Of course, for a given system of atoms, this is the reciprocal density. As bulk water consists of identical molecules represented by oxygen atoms, any type of Voronoi cells discussed above can be used in this case.

3.1.2. Voronoi Cell Volume Distribution. The dependence of the Voronoi cell volume of the water molecules as a function of the distance r from the solute molecule is shown in Figure 6.

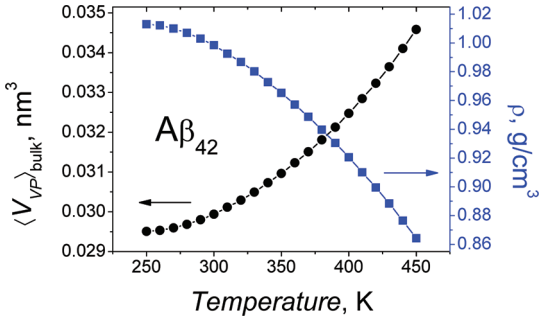

Figure 5. Density of bulk water in Aβ42 solutions (squares, right axis) and the mean volume of the Voronoi cells of these water molecules (circles, left axis).

S-cells are used here to take into account the different sizes of solute (heavy) atoms and water (which is represented by the oxygen). To calculate the Voronoi volume V_S at a distance r, we average over all water molecules whose oxygen atom is found in the layer between r and r + dr, and then the averaging over configurations of the simulation run was performed, as in the calculations of $\rho(r)$ in Figure 4. The first peak and following oscillations in Figure 6 are much less pronounced than in Figure 4, and the curves flatten out to the bulk limits at smaller values of r.

Comparing Figures 4 and 6, it has to be kept in mind that the underlying averaging processes cover slightly different regions: whereas $\rho(r)$ reflects the number of water oxygen atoms, found in small shells, the Voronoi cells of these atoms extend further out (see discussion in section 3.3). Therefore, the Voronoi cell volume distribution is smoother, but an overall reciprocal behavior can be observed. At small distances in Figure 6 (below about 0.2 nm), the Voronoi cell volumes are smaller than the bulk average. These molecules belong to the first peak in $\rho(r)$ of Figure 4, where a denser packing of the molecules is present, with the water molecules closest to the solute molecule having the smallest Voronoi cells. The subsequent region in Figure 6 with positive deviation from the bulk value comprises water molecules which extend into the region of the first minimum in $\rho(r)$, where the solvent molecules are less crowded.

Figure 7 shows the mean volumes of the Voronoi cells in successive Voronoi shells (illustrated in Figure 2). Instead of a continuous variable r, now we have discrete values k for the sequence of Voronoi shells. The restriction to five Voronoi shells is due to the fact that the following ones are influenced by the

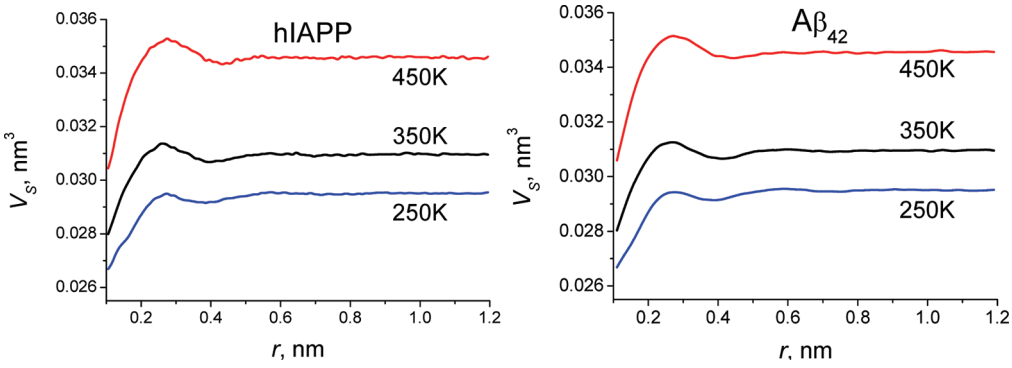

Figure 6. Average Voronoi cell volume of water molecules at distance r from the solute molecule for hIAPP and Aβ42. r is, as before, the distance between the water oxygen center and the surface of the nearest heavy atom of the solute molecule.

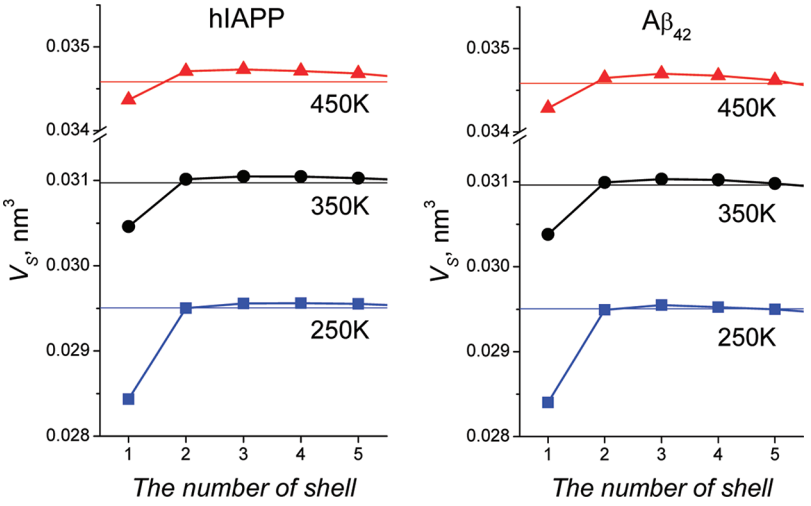

Figure 7. The mean Voronoi cell volume of water molecules in Voronoi shells as a function of the number of the shell for hIAPP and Aβ42 solutions. Horizontal lines indicate the mean Voronoi cell volume of the bulk water.

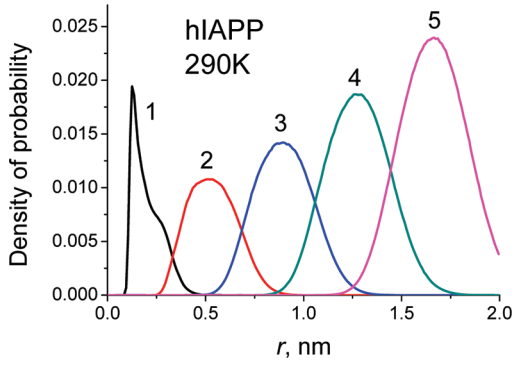

Figure 8. Distance distribution of water molecules in successive Voronoi shells number 1−5 around the hIAPP molecule in solution.

periodic boundary conditions of the simulation. The mean Voronoi cell volume was calculated here over water molecules of a given shell, and then the averaging over different configurations of the model was performed. This distribution is even more smoothed out in comparison to Figure 6.

As one can see, the mean volume of the cells in the first Voronoi shell is appreciably smaller than in the following ones, in agreement with the data in Figure 6. In Figure 8, the distance distribution of the water molecules within the Voronoi shells is shown. The maximum of the first distribution is positioned at 0.15 nm. This corresponds to the first peak of $\rho(r)$ in Figure 4, a shell of dense packing. Accordingly, the maximum of the first distribution is positioned at the left slope of the curve in Figure 6, where we localized the smallest cell volumes.

Note, the distribution of water molecules in the Voronoi shells (Figure 8) is rather broad. There is a substantial overlap between neighboring shells; e.g., there are many water molecules which belong to the third Voronoi shell but have a smaller distance to the surface of the solute molecule than some members of the second shell. Thus, the Voronoi shell method and the distance based criteria are not equivalent in selecting solvation shells; they encompass different sets of the solvent molecules.

A principal feature of the curves in Figure 7 is that they do not reach the asymptotic values of bulk water; in particular, water molecules of the third Voronoi shell, located mainly in the interval from 0.6 to 1.2 nm, see Figure 8. At these distances, the distributions in Figures 4 and 6 have already reached the asymptotic values, especially at high temperatures. However, the mean Voronoi cell volume in the third shell exceeds the asymptotic value for each temperature (compare the horizontal line in Figure 7).

dx.doi.org/10.1021/jp2050788 |J. Phys. Chem. B 2011, 115, 14217–14228

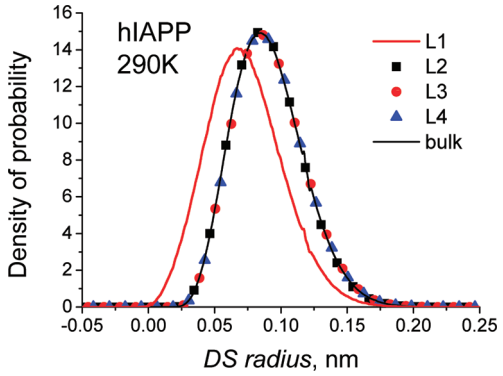

Figure 9. Distribution of radii R_{DS} of the inscribed spheres of Delaunay simplexes in different simplicial layers L1−L4 around hIAPP. Red curve, first layer; symbols, second to fourth layer; black curve, bulk.

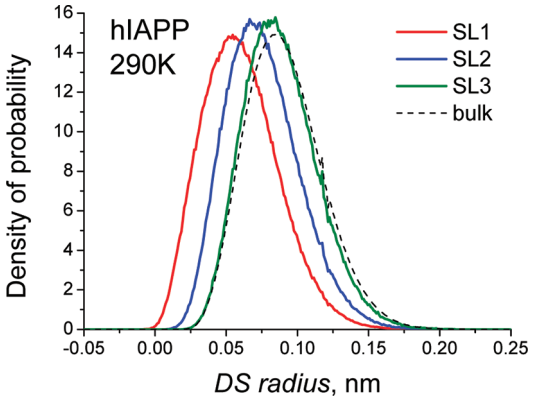

Figure 10. R_{DS} - distributions for different sublayers of the first simplicial layer around hIAPP in aqueous solution. Red, first sublayer; blue, second sublayer; green, third sublayer; dashed black, Delaunay simlexes of bulk water.

Moreover, the discrepancies become larger at higher temperatures. This seemingly contradictory behavior is however the result of a general geometrical property of a mosaic, of Voronoi tessellation in our case. It is known from general mathematical considerations that for any nonregular mosaic there is a positive correlation between the cell volume and the number of its neighbors: the bigger the cell, the larger the number of its neighbors. This assigns the larger cells a larger weight in the averaging process and means that even in pure liquids the mean value of the Voronoi cell volume, averaged over a given Voronoi shell around an arbitrarily chosen molecule (see Figure 2 for illustration), is not equal to the mean volume calculated over the entire system. In other words, a shell on a mosaic is not a representative subset for the calculation of the mean volume of a cell for the entire mosaic (a detailed discussion of this phenomenon and its correction can be found in refs 42 and 56). This effect is rather small, and it does not matter for the selection of neighbor atoms; however, it should be taken into account in the calculation of volumetric characteristics; see section 3.2 below.

3.1.3. The Hydration Shell Structure, as Described by Simplicial Layers. The results presented above suggest that our solute molecules do not change the water structure at larger distances. Changes can be detected in the nearest surroundings only. In particular, when we consider the volumetric and geometric characteristics of the Voronoi cells of the water molecules, we find that only the first Voronoi shell exhibits marked differences from bulk water. An analysis of the simplicial layers, introduced in Figure 3b, gives the same results: specific deviations from the bulk water structure can be found only in the first simplicial layer. Figure 9 gives the distribution of the inscribed radii R_{DS} inside the Delaunay simplexes of consecutive simplicial layers, from the first to the fourth one, for the hIAPP solution.

A clear deviation is visible for the first layer distributions, whereas the distributions for the next simplical layers are indistinguishable within the accuracy of our analysis. Obviously, the divergence of the first simplical layer is largely due to geometrical reasons: the "hard cores" of the solute atoms impose spatial restrictions.

As mentioned in conjunction with Figure 3, the simplexes of the first layer can be distinguished by their vertexes. Each simplex has four vertexes, and accordingly different species of simplexes are possible: (i) three vertexes are formed by atoms of the solute molecule and one by the oxygen of a water molecule, (ii) two vertexes are solute atoms and two are water oxygens, and (iii) one vertex is on the solute and three are in water. In other words, the first simplicial layer can be divided into three *sublayers,* each of them consisting of simplexes of type i−iii. We call them SL1−SL3 accordingly.

Figure 10 demonstrates the distributions of the inscribed sphere radii for the sublayers of the first simplicial layer L1 shown in Figure 9. There is a significant difference between the first, second, and third sublayers, the third coinciding with bulk water. Thus, the distinction of the first simplicial layer from the others, shown in Figure 9, is caused purely by the special features of the first and second sublayers.

3.2. Apparent Volume of Solute Molecule. The *apparent* volume of the solute molecule, V_{app}, is the difference between the volume of the solution containing a single molecule and the pure solvent (the partial molar volume of the solute at infinite dilution). Usually this volume is subdivided into

$$V_{app} = V_{int} + \Delta V \quad (1)$$

where V_{int} is the *intrinsic* volume of the solute molecule and ΔV is the *contribution of the hydration water* to the apparent volume, originating from the density change in the surrounding water, which is caused by the influence of the solute molecule. Working with computer models, it is in principle possible to calculate all mentioned volumetric parameters. However, this is not trivial. We will calculate the apparent volume by three different methods and compare the results of a traditional distance based approach with the results obtained by two variants of the Voronoi−Delaunay method.

The apparent volume of a solute molecule can be calculated by

$$V_{app} = V_{tot} - V^{h}_{bulk\_water} \quad (2)$$

Here, V_{tot} means the *total* volume occupied by the solute molecule and the water molecules in the hydration region, which includes all water molecules which are influenced by the presence of the solute. $V^{h}_{bulk\_water}$ is the volume of the same number of water molecules in pure (bulk) water. Formulas 2 and 1 are identical because $V_{tot} = V_{int} + V^{h}$ and $\Delta V = V^{h} - V^{h}_{bulk\_water}$, where V^{h} is the volume of the hydration region.

The traditional approach to define the hydration region implies an outer surface of the region at a distance R from the solute molecule (Figure 11). Usually this surface is chosen as the locus of points equidistant from the van der Waals surfaces of the

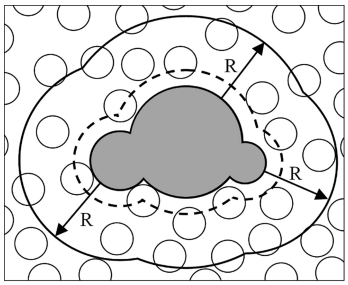

Figure 11. Illustration of the hydration region around a solute molecule, selected by a distance based (DB) criterion. Outer border is the surface of the union of spheres which are located on the atomic centers of the solute molecule and have radii $R_{vdW} + R$ (R_{vdW}: atomic van der Waals radius). Dashed line shows the surface at a distance R, which is equal to the radius of the solvent molecule (the so-called "solvent accessible surface" SAS).

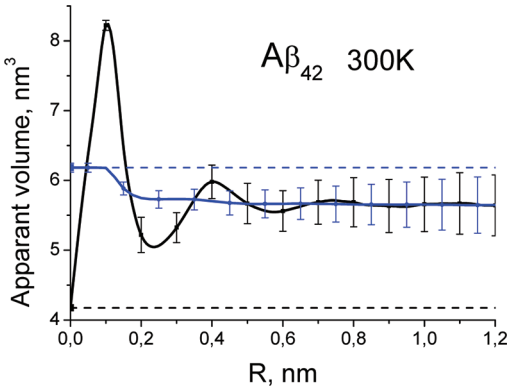

Figure 12. Apparent volume of Aβ42 in water as a function of R (extension of the hydration region). The black line was calculated by the traditional approach, using a DB criterion (Figure 11). The blue line was calculated using the DB criterion in combination with the volumes of the Voronoi cells (Figure 13). The lower dashed horizontal line indicates the van der Waals volume of the solute molecule ($R = 0$). The upper dashed horizontal line corresponds to the Voronoi volume of the molecule (here: sum of molecular Voronoi S-cells). Vertical lines show the standard deviation of the calculated values.

atoms of the solute molecule. The total volume inside such a surface can be calculated as the volume of the union of spheres of corresponding radii $R_{vdW} + R$, located on the atomic centers of the solute molecule (where R_{vdW} is the van der Waals radius of the atoms).

As the solute molecule can consist of a large number of atoms and the corresponding spheres have multiple overlapping, such calculations are involved and time-consuming. However, this problem has been treated mathematically in a general way,[24,57−59] and there are several programs available for the calculation of such volumes.[59−61] Here, we used our own software, which is rather fast and robust.[62] This is important when analyzing thousands of molecular dynamic configurations for a series of R values each.

To determine V_{app} according to eq 2, the total volume $V_{tot}(R)$ was calculated for a sequence of R values from 0 to 1.2 nm with steps of $\Delta R = 0.02$ nm. The number of water molecules inside every R-surface $N^h(R)$ was counted, and the value of $V^h_{bulk\_water}$ for each hydration region was estimated as

$$V^h_{bulk\_water} = N^h(R)v_0 \quad (3)$$

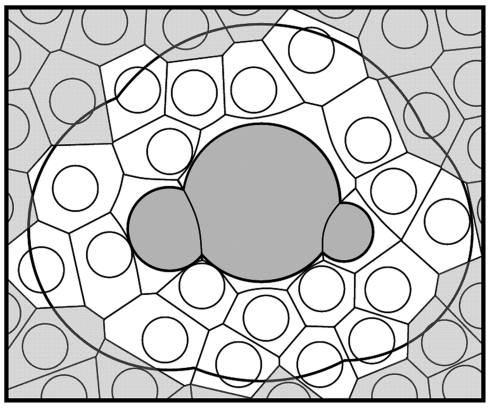

Figure 13. Estimation of the volume $V_{tot}(R)$ inside a hydration region around a solute molecule with the help of Voronoi cells: summing the Voronoi cell volumes of all atoms, whose centers lie inside the shell, including the solute and solvent molecules (Voronoi cell summation with DB criterion).

where v_0 is the mean volume occupied by a water molecule in bulk water.

Figure 12 (solid black line) illustrates for the case of the Aβ42 molecule in solution at 300 K the dependence of the obtained apparent volume as a function of the distance R. A strong first peak and the following oscillations of this function show similarity to Figure 4, where the density distribution function $\rho(r)$ is presented. The other temperatures show an analogous behavior. The required value of the apparent volume corresponds to the asymptotic value of this function, which is reached after about 0.8 nm in this case. Strong deviations of the function from the asymptotic value for smaller R reflect the structure of the hydration region and are not related to the real apparent volume. These oscillations can be an origin of error if one choses an inappropriate value of R. In particular, the error for the apparent volume will be approximately 6% of the real value if we take $R =$ 0.4 nm. On the other hand, to use larger values of R is also not advisible, because of an increase of inaccuracy (see error bars), which is due to the fact that the apparent volume is calculated as the difference between two large numbers, which are growing fast with R, see eq 2. The apparent volume also fluctuates strongly with time; obviously, it is sensitive to the conformation of the solute molecule. (Fluctuations of the radius of gyradion R_G and the SAS area have been analyzed in ref 21.) Standard deviations of the calculated values of V_{app} are shown by vertical lines in Figure 12.

Figure 12 shows also the apparent volume calculated in a different way. Using the same R-surfaces around the solute, we estimated the volume $V_{tot}(R)$ as the sum of the Voronoi cells of all atoms, whose centers lie inside this surface, i.e., of the solute molecule and of the hydration water molecules (illustrated in Figure 13). This method for estimation of V_{tot} is reasonable, as by definition a Voronoi cell represents the volume assigned to a given atom. Thus, the calculated sum is the volume assigned to all atoms inside the R-surface. The corresponding volume of the hydration water molecules in pure water was calculated as in eq 3.

The coincidence of the asymptotic values of both curves in Figure 12 emphasizes the accuracy and reliability of our calculations. One can see an obvious advantage of the second method in comparison with the traditional one: there are no strong oscillations in $V_{app}(R)$, and the asymptote is reached sooner. In particular,

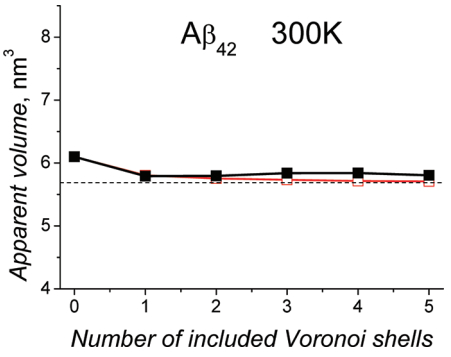

Figure 14. Apparent volume of Aβ42 in aqueous solution, calculated by summing over an increasing number of Voronoi shells. Full squares, without corrections; empty squares, with corrections (see text). The horizontal line indicates the asymptotic value of the apparent volume in Figure 12. The volume of shell number zero corresponds to the intrinsic volume of the solute molecule (section 3.3).

even with $R = 0.2$ nm, the deviation of the apparent volume from the asymptotic value is less than 2% (Figure 12). This advantage is explained by the fact that each water molecule contributes to the shell with its full volume. This damps the oscillations, which originate from the behavior of $\rho(r)$.

Third, we calculate the apparent volume using the construction of *Voronoi shells* around the solute molecule; thus, instead of a continuous variable R, we consider now a discrete number of shells k. The value $V_{tot}(k)$ is defined as the average value of the sum of the Voronoi volumes of the water molecules in the Voronoi shells from the 1st to the kth one plus the Voronoi volume of the solute molecule itself. At first glance, the volume $V^{h}_{bulk\_water}$ of the same number of water molecules in the bulk can be calculated as in eq 3: as product $N(k)\cdot v_0$, where $N(k)$ is the average number of water molecules in the k Voronoi shells. However, as already mentioned in section 3.1.2, we have to take into account the fact that the mean volume of a Voronoi region in the bulk is not equal to the product of the mean number of Voronoi cells in the region $N(k)$ times the mean cell volume v_0 calculated for the entire system. The mathematical origin of this phenomenon was discussed elsewhere:[42,56] there is a correlation between cell volume and number of its neighbors in any disordered mosaic, which should be taken into account when calculating $V^{h}_{bulk\_water}$.

A semiempirical method to take this phenomenon into account was proposed in ref 42: A correction factor γ_k for each Voronoi shell can be determined. The factor γ_k takes into account characteristic geometric parameters of the kth Voronoi shell, namely, the numbers of outer and inner Voronoi faces of the shell, f_k and f_{k-1}. Those can be easily calculated at the determination of the shells. As a result, to calculate the subtrahend volume, eq 3 is replaced here by $V^{h}_{bulk\_water} = (n_1\gamma_1 + n_2\gamma_2 + \ldots + n_k\gamma_k)\cdot v_0$. n_k is the average number of water molecules found in Voronoi shell k. Figure 14 shows the apparent volume as a function of the number of included Voronoi shells for Aβ42 at 300 K. The values with and without consideration of the discussed correction are shown. The difference between the curves is not very large (3% for $k = 3$), but it should be taken into account, because the magnitude of the volume difference ΔV between apparent and intrinsic volume is also of the order of a few percent only.

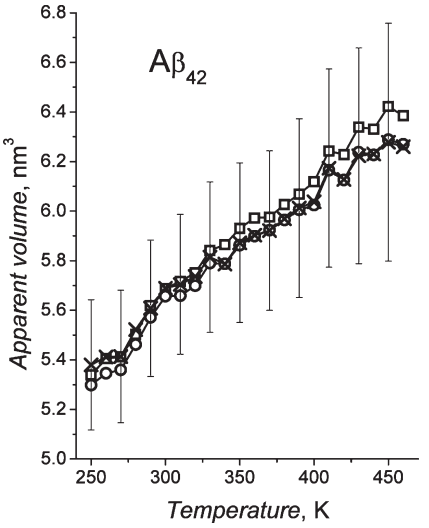

Figure 15. Apparent volume of Aβ42 as a function of temperature calculated by different methods: crosses, traditional method with DB criterion; circles, Voronoi volumes with DB criterion; squares, summation over Voronoi shells.

It seems that the mentioned property of the mosaics does not appear if we average the volume of Voronoi cells selected by the DB criterion (Figure 12). The Voronoi cells at a distance R can belong to different Voronoi shells; thus, a correlation between topology and metric of the Voronoi cells will not be so important.

Figure 15 shows the apparent volume of the Aβ42 molecule in aqueous solution as a function of temperature, calculated by all three methods discussed. The first and the second give practically the same values for the full temperature interval. The last one (with the corrections) gives also a reasonable agreement at low temperatures. However, differences become visible with increasing temperature.

3.3. Intrinsic Volume of the Solute Molecule. The determination of the *intrinsic* volume of biomolecules has been discussed in computational molecular biology for a long time.[2,39] There is not a unique solution: if we use a pure DB criterion, the result depends on the definition of the border between solute and solvent. As discussed in section 3.2, using $R = 0$, the van der Waals volume of the solute molecule is obtained. Another possibility is to use for R a value equal to the radius of the solvent molecule; this yields the volume inside the well-known solvent accessible surface SAS (Figure 11).

The Voronoi–Delaunay method seems to offer a well-defined solution of the problem. Although there is a lack of uniqueness, because there are different types of Voronoi tessellations (section 2.2), for volumetric problems, the S-tessellation apparently is the most suitable one. In this case, the volume assigned to each atom is defined in the most natural way. Power tessellation can be considered as a good approximation. It can be easily calculated and processed because power cells have flat faces unlike the S-cells. An ordinary Voronoi tessellation does not take into account the radii of the atoms and can be used for molecular systems only as an auxiliary geometrical tool.

In this paper, we use Voronoi S-tessellation and calculate the intrinsic volume V_{int} as the sum over the S-cells of all atoms of the solute molecule. Thereafter, the contribution of the hydration water ΔV can be obtained easily as the difference of V_{app} and V_{int} according to eq 1. Figure 16 summarizes the obtained volumetric

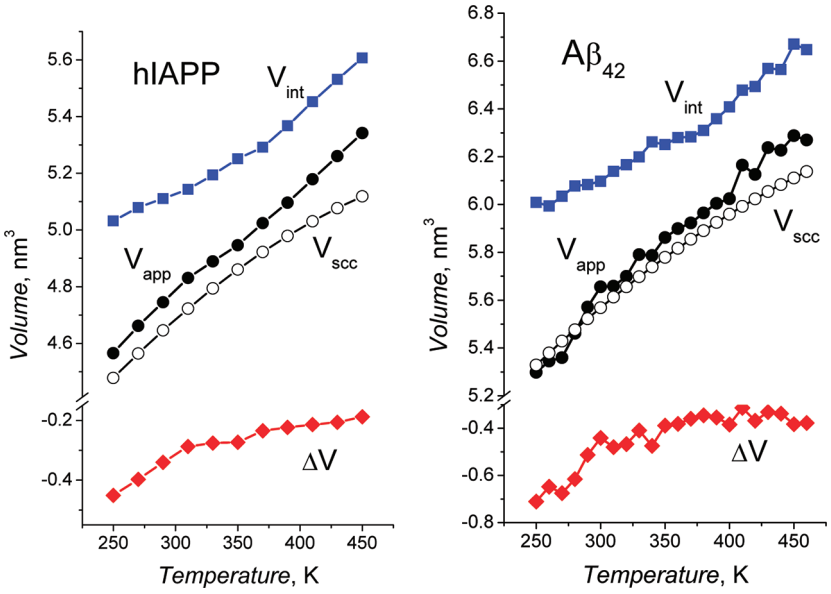

Figure 16. Intrinsic and apparent volumes and the contribution ΔV of the hydration water for hIAPP and Aβ42 molecules as a function of temperature. Intrinsic volume: sum over the *S*-Voronoi cells of all atoms of the solute molecule. Apparent volume: asymptotic value from summation of Voronoi cells within the DB criterion (section 3.3). ΔV: difference $V_{app} - V_{int}$. Empty symbols: V_{scc}, show the apparent volume calculated by the empirical amino acid side-chain contribution method of Haeckel et al.[63] (As emphasized by these authors, the parameters for V_{scc} had been determined for the limited temperature range 280−360 K and have to be considered less reliable outside.)

parameters (apparent and intrinsic volumes and contribution of hydration water) for the Aβ42 and hIAPP molecules as a function of temperature.

The apparent volume V_{app} shown in Figure 16 was determined as the asymptotic value (for large R) of the sum of Voronoi cell volumes within a given DB cutoff (see section 2.2 and Figure 12). Remember, it coincides with the result of the traditional methods (Figure 15). One can see that the apparent volume increases with temperature. From a logarithmic plot of V_{app}, we determined the thermal expansion coefficient $d\ln V/dT$. As in the study of Brovchenko et al.,[21,64] we observe a kink at about 320 K. The slopes below and above this temperature are 0.94×10^{-3} and 0.77×10^{-3} K^{-1}, respectively, for hIAPP and 1.15×10^{-3} and 0.69×10^{-3} K^{-1}, respectively, for Aβ42. The latter values are in good agreement with those obtained in ref 21.

The intrinsic volume V_{int} of both molecules is greater than their apparent volume by about 10% for all temperatures. As for V_{app}, the coefficient of thermal expansion of V_{int} is also positive for both molecules and shows a (less pronounced) kink in the temperature dependence at about 320 K. Note, if one considers the van der Waals volume as the intrinsic volume of the solute, it does not change with temperature and has a much lower value than the apparent volume (by about 30% for Aβ42 at 300 K, as shown in Figure 12).

Figure 16 shows the contribution ΔV, calculated as the difference of the apparent and intrinsic volumes. It is *negative* for our models, and the absolute value decreases with temperature. It has a positive slope, and the main change is observed in the temperature interval up to 320 K. There are at least two distinct structural reasons for this negative value of ΔV: electrostriction close to charged groups and a "filling" of the open structure (voids) of water[65,66] by the nonpolar side groups. A shrinking of the free volume in the first simplical layer around the solute molecule can be seen clearly as a pronounced shift of the distribution of the inscribed radii R_{DS} inside the Delaunay simplexes (Figures 9 and 10). This has to be studied in more detail in future work.

Here we face strong and qualitative differences compared to the results, obtained in a previous analysis of the same simulation runs for the Aβ42 solution: in ref 21, *positive* values for ΔV, and intrinsic volumes V_{int}, which are *decreasing* with temperature, thus showing negative intrinsic thermal expansion coefficients, were obtained. We explain these discrepancies by the two largely differing approaches to calculate these properties: whereas we calculate V_{app} and V_{int} directly from the simulation run via Voronoi constructions and get ΔV as the difference of these two data, in ref 21, ΔV is calculated from the density of the hydration shell water. This is determined by counting the water molecules within some distance D from the heavy atoms of the solute molecule (the assumed hydration shell) and dividing this number by the volume of the hydration shell, which is estimated as V_D = SASA·(D − solvent radius). As one can easily imagine, this latter step overestimates the appropriate volume when the chain is not stretched out, leading thus to a decreased density and thus to a positive volume contribution ΔV. Using our approach, based on the union of spheres, as discussed in conjunction with Figure 11, a more correct value of V_D could be obtained as the difference between the volumes of the overlapping spheres, indicated schematically by the full and dashed black lines in Figure 11.

Chalikian et al.[2] suggested to dissect changes in partial specific volume, and hence in the expansion coefficient α of a protein into essentially three different contributions: (1) the intrinsic volume, V_{intr}, which originates from the van der Waals volume of the constituent atoms plus the volume of intrinsic voids within the water-inaccessible protein interior, (2) a hydrational term, δV_{hydr}, also denoted "interaction volume", describing—with regard to the bulk solvent—changes of the solvent volume associated with the hydration of solvent-accessible protein atomic groups, i.e., from solute−solvent interactions around the charged (electrostriction), polar (hydrogen-bonding), and nonpolar (hydrophobic hydration)

atomic groups on the protein surface, and (3) the thermal volume, V_{therm}, which results from thermally induced mutual molecular vibrations and reorientations of the solute and the solvent. The effect of the thermal volume is to expand the solvent away from the surface of the protein, such that solvent-free volume elements form around the protein. Altogether, one obtains $V \approx V_{intr} + \delta V_{hydr} + V_{therm}$. In our approach, the thermal volume V_{therm} is not appearing explicitly but partitioned between V_{int} and ΔV. V_{therm} is considered to increase with temperature, leading to a positive contribution to the thermal expansion coefficient α, and hence to positive slopes of V_{int} and ΔV, as obtained from our calculations.

It is interesting to note that, despite the strong differences in ΔV and V_{int} between our results and those presented in ref 21, the values for V_{app}, although obtained in very different ways in both studies, coincide closely. In ref 21, V_{app} has been calculated simply as the volume difference between two simulation runs with and without one Aβ42 molecule. This agreement supports the reliability of both approaches, when calculating the "experimentally accessible" property V_{app}. The difficulties are in fact in the partitioning of the contributions ΔV and V_{int}.

The apparent volume V_{app}, obtained from the simulations, can be reproduced quite well by an empirical approximation, which allows a simple estimation of the partial molar volumes of polypeptides from the side-chain contributions of the primary amino acid sequence;[63] see empty circles in Figure 16. These values V_{scc} are calculated via eq 16 of ref 63 (with eqs 8, 17, and 18), applying the parameters from Tables 1 and 3 there. The parameters have been obtained by Haeckel et al. from partial molar volumes of tripeptides glycyl-X-glycine, measured in the temperature range from 280 to 360 K for all 20 amino acids X. In principle, this approach can only be applied to elongated chains. The coiling of the chains in the simulations leads to an increase of V_{app} compared to V_{scc}: when there are close contacts between side chains, hydration water with a *negative* contribution to V_{app} is eliminated and V_{app} increases, as can be seen in Figure 16. From the results of section 3.1.3, we can deduce that these contacts are efficiently influencing the volumetric properties only, when these contacts are close: the influence of the solute on the volumetric properties of the hydration water is restricted to the closest two simplicial sublayers; thus, no extended hydration shells are needed to develop fully the influence of the solute on the volumetric properties of the hydration water. In other words, we expect from our results that coiling or aggregation is visible only when direct contacts between side chains are present. This is in agreement with the results of a recent molecular dynamics study on the pressure denaturation of a protein:[68] these authors observed that, once the protein is sufficiently water swollen, the partial molar volume of the protein appears to be insensitive to further conformational expansion or unfolding. Another aspect of the negative sign of ΔV is furnished via Le Châtelier's principle: increasing pressure will favor less direct contacts and hence dissociation of protein aggregates. This is in fact observed experimentally.[67]

Clearly, the agreement between V_{app} and V_{scc} is much better for Aβ42 than for hIAPP. This is only fortuitous for the following reasons: in the simulations, Aβ42 contains six side chains with full charge −1e. As Haeckel et al. explain, in their measurements, which are used for the determination of the parameters for the residues D and E, these residues are only partly ionized. As these authors point out further, neutral side chains would lead to larger volumes; correspondingly, we conclude that side chains with charge −1e lead to smaller volumes in the simulations and this brings the data for V_{app} and V_{scc} into closer agreement. The negatively charged residues D and E are missing in hIAPP.

4. CONCLUSIONS

In this paper, we examined the applicability and the advantages of the Voronoi−Delaunay method to study the volumetric properties of large hydrated biomolecular systems such as proteins on the basis of simulation models. We apply this method to analyze the trajectories of molecular dynamics simulation runs of hIAPP and Aβ42, two polypeptides of high relevance for understanding the amyloidogenesis of peptides in aqueous solution. Voronoi tessellations are calculated on the basis of all heavy atoms of the model systems (excluding hydrogen). Both power (radical) tessellation and Voronoi *S*-tesselation (additively weighted in mathematical notation) were used to take into account the van der Waals radii of the atoms. The former one is easier to calculate, the latter has a more clear physical meaning of the volume assigned to the atoms.

One problem, which is arising in the investigation of hydration shells, is the assignment of neighboring or hydration water molecules around the solute. Usually this is done by using a distance based criterion, i.e., by selection of the molecules within the limits of some reasonably chosen distance R from the solute. The Voronoi−Delaunay method gives a nonambiguous alternative approach. It defines the neighbors without any auxiliary parameters. Moreover, it provides a clear-cut method to select successive shells of the solvent molecules around the solute (the first, second, and following Voronoi shells). Using Delaunay tessellation, which is dual to the Voronoi one, it is possible to yield an even more detailed resolution of the environment of a solute molecule. Delaunay simplexes allow the division of every Voronoi shell into Delaunay sublayers. The analysis of consecutive Voronoi shells demonstrated that the essential *volumetric* difference between hydration water and bulk water is observed only in the nearest neighborhood of the solute, practically in the first two Delaunay sublayers of the first Voronoi shell.

To calculate the apparent volume of the solute molecule, one has both to specify the hydration water and to calculate its volume. Different methods for the determination of the apparent volume were tested: (i) a traditional one, using an exclusively distance based criterion, (ii) a combination of a distance-based criterion with Voronoi cells, and (iii) using Voronoi shells on the Voronoi tessellation. Some computational aspects of the methods were discussed. We could show that all of them give practically the same results if they are used correctly. However, from our experience, method ii should be preferred, as it shows fast convergence and is less prone to the influence of Voronoi cell volume correlations within the Voronoi mosaic, which has to be corrected subsequently.

To decompose the apparent volume into the intrinsic volume and the contribution of the change in the hydration water density, we determined the intrinsic volume V_{int} by the Voronoi approach. In the frame of the traditional, purely distance based method, there is some arbitrariness concerning the localization of the border between solute and solvent. In the frame of the Voronoi−Delaunay method, the intrinsic volume of the solute molecule can be defined as the Voronoi volume of the molecule, i.e., the sum of the Voronoi cells of all atoms of the solute molecule. We used the Voronoi *S*-tessellation which seems more appropriate for the assignment of individual volumes to atoms with different van der Waals radii. We found that the intrinsic

volume of both solute molecules is greater than their apparent volume by about 10%. This means that the contribution of the hydration water is *negative*, and the surrounding water is denser than in the bulk.

Our results have been compared with the quasi-experimental side chain contribution data of Haeckel et al.[63] for elongated peptide chains. A reasonable agreement demonstrates the reliability of our calculations. The observed differences could be explained by the coiling of the chains and the resulting geometric contacts between the residues. This indicates also the sensitivity of volumetric studies and helps to understand the pressure denaturation of proteins and the pressure dependence of the partial molar volumes.

Our results were obtained by averaging over a large number of configurations of the simulation runs. We could see that the volumetric characteristics vary strongly with the shape of the solute molecule. Different residues of the peptide chain have a different influence on the surrounding water, and this influence is modified by fluctuating interactions between them. Such questions have to be studied in detail in subsequent work. We may expect, in the near future, that this method will show its great potential also in studies of proteins involved in folding and intermolecular interactions, which are largely controlled by hydration effects.[13]

AUTHOR INFORMATION

Corresponding Author

*E-mail: nikmed@kinetics.nsc.ru (N.N.M.); alfons.geiger@udo.edu (A.G.).

ACKNOWLEDGMENT

Financial support from Alexander von Humboldt foundation, RFFI grant 08-03-00140, and Deutsche Forschungsgemeinschaft (DFG) is gratefully acknowledged.

REFERENCES

(1) Royer, C. A. *Biochim. Biophys. Acta* **2002**, *1595*, 201–209.
(2) Chalikian, T. V. *Annu. Rev. Biophys. Biomol. Struct.* **2003**, *32*, 207–235.
(3) Seemann, H.; Winter, R.; Royer, C. A. *J. Mol. Biol.* **2001**, *307*, 1091–1102.
(4) Rösgen, J.; Hinz, H.-J. *Biophys. Chem.* **2000**, *83*, 61–71.
(5) Ravindra, R.; Winter, R. *ChemPhysChem* **2003**, *4*, 359–365.
(6) Mitra, L.; Rouget, J. B.; Garcia-Moreno, B.; Royer, C. A.; Winter, R. *ChemPhysChem* **2008**, *9*, 2715–2721.
(7) Lin, L. N.; Brandts, J. F.; Brandts, J. M.; Plotnikov, V. *Anal. Biochem.* **2002**, *302*, 144–160.
(8) Ravindra, R.; Winter, R. *ChemPhysChem* **2004**, *5*, 566–571.
(9) Mitra, L.; Smolin, N.; Ravindra, R.; Royer, C.; Winter, R. *Phys. Chem. Chem. Phys.* **2006**, *8*, 1249–1265.
(10) Schweiker, K. L.; Fitz, V. W.; Makhatadze, G. I. *Biochemistry* **2009**, *48*, 10846–10851.
(11) Ravindra, R.; Royer, C.; Winter, R. *Chem. Phys. Phys. Chem.* **2004**, *6*, 1952–1961.
(12) Sirotkin, V. A.; Winter, R. *J. Phys. Chem. B* **2010**, *114*, 16881–16886.
(13) Zhai, Y.; Okoro, L.; Cooper, A.; Winter, R. *Biophys. Chem.* **2011**, *156*, 13–23.
(14) Lounnas, V.; Pettitt, B. M. *Proteins: Struct., Funct., Genet.* **1994**, *18*, 133–147.
(15) Vaisman, I. I.; Brown, F. K.; Tropsha, A. *J. Phys. Chem.* **1994**, *98*, 5559–5564.
(16) Merzel, F.; Smith, J. C. *Proc. Natl. Acad. Sci. U.S.A.* **2002**, *99*, 537853–83.
(17) Henchman, R. H.; McCammon, A. M. *Protein Sci.* **2002**, *11*, 2080–2090.
(18) Paschek, D. *J. Chem. Phys.* **2004**, 10605–10617.
(19) Schröder, C.; Rudas, T.; Boresch, S.; Steinhausera, O. *J. Chem. Phys.* **2006**, *124*, 234907.
(20) Smolin, N.; Daggett, V. *J. Phys. Chem. B* **2008**, *112*, 61936202.
(21) Brovchenko, I.; Burri, R. R.; Krukau, A.; Oleinikova, A.; Winter, R. *J. Chem. Phys.* **2008**, *129*, 195101.
(22) Okabe, A.; Boots, B.; Sugihara, K.; Chiu, S. N. *Spatial Tessellations: Concepts and Applications of Voronoi Diagrams*; Wiley: Chichester, U.K., 2000.
(23) Medvedev, N. N. *The Voronoi—Delaunay Method in the Structural Investigation of Non-crystalline Systems*; SB RAS: Novosibirsk, Russia, 2000 (in Russian).
(24) Edelsbrunner, H. *Discrete Comput. Geom.* **1995**, *13*, 415–440.
(25) Alinchenko, M. G.; Anikeenko, A. V.; Medvedev, N. N.; Voloshin, V. P.; Mezei, M.; Jedlovszky, P. *J. Phys. Chem. B* **2004**, *108*, 19056–19067.
(26) Poupon, A. *Curr. Opin. Struct. Biol.* **2004**, *14*, 233.
(27) Kim, D.-S.; Seo, J.; Kim, D; Ryu, L.; Cho, C.-H. *Comput.-Aided Des.* **2006**, *38*, 1179–1191.
(28) David, E. E.; David, C. W. *J. Chem. Phys.* **1982**, *76*, 4611–4614.
(29) Voronoi, G. F. *J. Reine Angew. Math.* **1909**, *136*, 67–179.
(30) Delaunay, B. N. *Proc. Math. Congr. Toronto, Aug 11—16, 1924*, 1928, 695—700.
(31) Mezei, M. *Mol. Simul.* **1988**, *1*, 327–332.
(32) Gellatly, B. J.; Finney, J. L. *J. Mol. Biol.* **1982**, *161*, 305–322.
(33) Procacci, P.; Scateni, R. *Int. J. Quantum Chem.* **1992**, *42*, 1515–1528.
(34) Raschke, T. M.; Levitt, M. *Proc. Natl. Acad. Sci. U.S.A.* **2005**, *102*, 6777–6782.
(35) Sterpone, F.; Marchetti, G.; Pierleoni, C.; Marchi, M. *J. Phys. Chem. B* **2006**, *110*, 11504–11510.
(36) Schröder, C.; Neumayr, G.; Steinhauser, O. *J. Chem. Phys.* **2009**, *130*, 194503.
(37) Bouvier, B.; Gruberg, R.; Nilges, M.; Cazals, F. *Proteins: Struct., Funct., Bioinf.* **2009**, *76*, 677–692.
(38) Neumayr, G.; Rudas, T.; Steinhauser, O. *J. Chem. Phys.* **2010**, *133*, 084108.
(39) Paci, E.; Marchi, M. *Proc. Natl. Acad. Sci. U.S.A.* **1996**, *93*, 11609–11614.
(40) Paci, E. *Biochim. Biophys. Acta* **2002**, *1595*, 185–200.
(41) Marchi, M. *J. Phys. Chem. B* **2003**, *107*, 6598–6602.
(42) Voloshin, V. P.; Anikeenko, A. V.; Medvedev, N. N.; Geiger, A.; Stoyan, D. *Proc.7-th Int. Symp. on Voronoi Diagrams in Science and Engineering, Quebec, 28—30 June 2010*; Quebec, Canada, 2010, 254—259.
(43) van der Spoel, D.; Lindahl, E.; Hess, B.; Groenhof, G.; Mark, A. E.; Berendsen, H. J. C. *J. Comput. Chem.* **2005**, *26*, 1701.
(44) Voet, D.; Voet, J. G. *Biochemistry*, 3rd ed.; John Wiley & Sons: Hoboken, N.J., 2004.
(45) Jorgensen, W. L.; Maxwell, D. S.; Tirado-Rives, J. *J. Am. Chem. Soc.* **1996**, *118*, 11225–11236.
(46) Kaminski, G.; Friesner, R.; Tirado-Rives, J.; Jorgensen, W. L. *J. Phys. Chem. B* **2001**, *105*, 6474–6487.
(47) Berendsen, H. J. C.; Grigera, J. R.; Straatsma, T. P. *J. Chem. Phys.* **1987**, *91*, 6269.
(48) Andrews, M. N.; Winter, R. *Biophys. Chem.* **2011**, *156*, 43–50.
(49) Oleinikova, A.; Smolin, N.; Brovchenko, I.; Geiger, A.; Winter, R. *J. Phys. Chem. B* **2005**, *109*, 1988–1998.
(50) Brovchenko, I.; Paschek, D.; Geiger, A. *J. Chem. Phys.* **2000**, *113*, 5026–5036.
(51) Anishchik, S. V.; Medvedev, N. N. *Phys. Rev. Lett.* **1995**, *75*, 4314–4317.
(52) Medvedev, N. N.; Voloshin, V. P.; Luchnikov, V. A.; Gavrilova, M. L. *J. Comput. Chem.* **2006**, *27*, 1676–1692.
(53) Aurenhammer, F. *SIAM J. Comput.* **1987**, *16*, 78–96.
(54) Oleinikova, A.; Brovchenko, I.; Winter, R. *J. Phys. Chem. C* **2009**, *113*, 11110–11118.

(55) Harrington, S.; Poole, P. H.; Stanley, H. E. *J. Chem. Phys.* **1997**, *107*, 7443.
(56) Weiss, V. *Stochast. Stochast. Rep.* **1995**, *55*, 295.
(57) Sastry, S; Corti, D. S.; Debenedetti, P. G.; Stillinger, F. H. *Phys. Rev. E* **1997**, *56*, 5524–5532.
(58) Liang, J.; Edelsbrunner, H.; Fu, P.; Sudhakar, P. V.; Subramaniam, S. *Proteins: Struct., Funct., Genet.* **1998**, *33*, 1–17. Ryua, J.; Parka, R.; Kim, D.-S. *Comput.-Aided Des.* **2007**, *39*, 1042–1057.
(59) Cazals, F.; Kanhere, H.; Loriot, S. *ACM Trans. Math. Software* **2011**, *38*, in press.
(60) Edelsbrunner, H.; Koehl, P. In *MSRI Publications - Vol. 52: Combinatorial and Computational Geometry;* Goodman, J. E., Pach, J., Welzl, E., Eds.; Cambridge University Press: Cambridge, U.K., 2007; pp 243−275.
(61) Till, M.; Ullmann, G. *J. Mol. Model.* **2010**, *16*, 419 .
(62) Voloshin, V. P.; Anikeenko, A. V.; Medvedev, N. N.; Geiger, A. *Proc. of 8-th Int. Symp. on Voronoi Diagrams in Science and Engineering, 28−30 June 2011, China*; Quingdao, China, 2011 (in press).
(63) Haeckel, D.; Hinz, H.-J.; Hedwig, G. R. *Biophys. Chem.* **1999**, *82*, 35.
(64) Brovchenko, I.; Andrews, M. N.; Oleinikova, A. *Phys. Chem. Chem. Phys.* **2010**, *12*, 4233–4238.
(65) Geiger, A.; Mausbach, P.; Schnitker, J. In *Water and Aqueous Solutions*; Neilson, G. W., Enderby, J. E., Eds.; Adam Hilger: Bristol, U.K., 1986; pp 15−30.
(66) Voloshin, V. P.; Medvedev, N. N.; Naberukhin, Yu.I.; Geiger, A.; Klene, M. *J. Struct. Chem.* **2005**, *46*, 451–458.
(67) Mishra, R.; Winter, R. *Angew. Chem., Int. Ed.* **2008**, *47*, 6518–6521.
(68) Sarupria, S.; Ghosh, T.; Garcia, A. E.; Garde, S. *Proteins: Struct., Funct., Bioinf.* **2010**, *78*, 1641–1651.